IJBPAS, November, Special Issue, 2021, 10(11): 924-935
ISSN: 2277–4998

International Journal of Biology, Pharmacy and Allied Sciences (IJBPAS)
'A Bridge Between Laboratory and Reader'

www.ijbpas.com

STRIP LESS VLSI INTEGRATED SELF-MANAGEABLE DEVICE FOR INTELLIGENT BLOOD GLUCOSE CONTROL ON DIABETES PATIENTS HEALTHCARE

K.SIVANANDAM[1*], R. MURUGASAMI[2], MALARVIZHI MANICKAM[3], SAKTHIVEL.S[4], SANKARA GOMATHI.S[5] AND DHARMBIR SINGH[6]

1: Associate Professor, Department of Electronics and Communication Engineering, M.Kumarasamy College of Engineering, Thalavapalayam, Karur -639113, Tamilnadu, India

2: Associate Professor, Department of ECE, Nandha Engineering College, Erode-638052, Tamilnadu, India

3: Assistant Professor in Chemistry at Sri GVG Visalakshi College for Women, Udumalpet, Tiruppur District, Tamil Nadu, India

4: Student in Biotechnology at Sri Venkateswara College of Engineering, Pennalur, Sriperumbudur, Kancheepuram District, Tamilnadu, India

5: Professor in Electronics and Communication Engineering at Adhi College of Engineering and Technology, Near Walajabad, Kancheepuram District, Tamilnadu, India

6: Professor at Maharishi Markandeshwar University, Ambala-134007, Haryana, India

***Corresponding Author: K.Sivanandam; E Mail: sivanandamk.ece@mkce.ac.in**

Received 22nd July 2021; Revised 25th Aug. 2021; Accepted 30th Sept. 2021; Available online 1st Nov. 2021

https://doi.org/10.31032/IJBPAS/2021/10.11.1080

ABSTRACT

To tackle the limitations of existing rigorous integrated care, an actual screen or semi-synthetic glycemic level tracking device is mentioned, such as discomfort while pricking, uncomfortable testing kits, and infection risks. The hypothesized anatomical testator has a rapid and precise authority on plasma and glycemic control, as well as bloodstream densities in dopaminergic blood, culminating in better metabolic monitoring. Additionally, the findings are processed to extract substantial random noise before being displayed on the actual display panel.

The device will use IoT to deliver precise data and send automatic alerts, avoiding undesirable events caused by severe changes in blood sugar levels. A pulsed laser diode, a photovoltaic sensor, a reduced noise amplifier, The framework comprises a more capable analog to the digital comparator (ADC), a microcontroller grid (FPGA), and an LCD. The frequency range and transmission ratio have been calibrated. The algorithm is constructed with FPGA and achieves maximum efficiency and security while utilizing little energy.

Keywords: Random noise; Coherence aggregating; Diabetes mellitus; Maximum transmit diode; Reduced noise transistor; ADC; Diabetes mellitus; Healthcare

INTRODUCTION

The human body's permissible average blood glucose level is 70mg/dl to 140mg/dl **[1]**. The beta pancreas produces secrete adrenaline to keep hyperglycemia in equilibrium. During the transformation of organic to insulin, the reaction can take place in the circulatory system. The hormonal problem occurs in the human body when there is a glucose shortage, insulin sensitivity, or both **[2, 3]**. Types 1 and 2 diabetics are the two most common kinds of diabetes mellitus recognized in clinical practice. The WHO recommends 126mg/dl overnight and 200mg/dl 2 hours after consuming 75g of maltose for type 1 or type 2 hyperglycemia. Type 1 hyperglycemia occurs when the cell generates insufficient doses of glycogen or no insulin at all. In this predicament, one's own body's lymphocytes unexpectedly attack beta cells, leading to blood sugar buildup **[4]**. To maintain constant insulin levels, this ailment can be managed with hormones or adequate meal preparation.

Type 2 diabetes mellitus originates is when a person's body is unable to metabolize the produced insulin and demonstrates a diminished sensitivity. It can be handled using physical exercise, diet modification, and pharmaceuticals, or insulin shots. The metabolic derangement is associated with the high concentration in hyperglycemia which is not absorbed as metabolism. Progressive kidney sickness, ophthalmology, the elevated likelihood for cardiovascular diseases, impaired neurological transmission, gestational diabetes in women who are pregnant Frustration, chronic health issues, and semi extremity potation all appear to be tangible effects (further than 140mg/dl, 7.8mmol/l). Disorientation, unconsciousness, and mortality are some of the consequences of hypoglycemia (low blood sugar levels) **[6]**. To prevent the aforementioned complications, the quantity of

glycemic in the immune system must be monitored, especially in diabetes patients. The sensitive and nonmethods of monitoring hyperglycemia are used **[7]**. Expensive surgeries are uncomfortable because they require poking the finger to acquire blood tests. They also provide a danger of infection and, in the medium term, harm to the knuckle tissue. This method is also expensive because it requires the use of a fresh strip every occasion the insulin levels have to be examined **[8]**.

However, there has been a shift toward semi inspections that helps to mitigate the disadvantages of more aggressive treatment. Using retinal or percutaneous means, the molecule of glucose has been given the authority to interface with physiochemical mechanisms in the bloodstream in semi techniques **[9]**. Frustration, hyperpigmentation, and scorching are common side effects of permeation methods. Spectral methods are used to tackle the issue with subcutaneous methods **[10]**. Laser heat is transferred to acoustic energy through assimilation in the image process, resulting in energy radiation and perceptible amplitude modulation. An acoustic piezoresistive detects acoustic waves generated by surface tension in the skin **[11]**. In this demonstration, a piezoelectric transducer is used to predict compression waves and convert them to nerve impulses.

Related Works

An epidermis, mesoderm, and hypodermis are the three anatomical layers of human skin, germinal epithelium, lamina propria, superficial fascia, squamous epithelium hypodermis, and the topmost endothelium are some of the layers that make up an epidermis. The endothelium has a consistency of 10-20m, while the remainder of the epithelial is 0.1-0.3 mm wide. The epidermis is 1-2 mm wide, while the submucosa is 2-4 mm wide. Its wider capillaries have been predicted within submucosa, whereas this integument encompasses a myriad of glomerular capillaries **[12]**. An epidermis constitutes numerous 20% of the body's solvent, with the endothelium being the costliest and the integumentary system consisting approxi-mately 60% of the quantity of water serum concentrations are investigated in organic molecules, the susceptibility depth of semi-light is reduced below 100m because to considerable hydration. Its district and sub photons rarely penetrate the vasculature and capillaries due to the obvious significant hydration. Its plasma glucose level must be ascertained in the interstitium (ISF) of the abdominal area rather than through plasma

[13]. As glycogen diffusion occurs predominantly through all the ISF, hyperglycemia calibration on the ISF has been shown to illuminate hyperglycemia **[14]**.

In another designed framework, a synchrotron diode (PLD) component oscillating at 905 nm and 1550 nm is utilized. Fructose has the highest concentration at this frequency of 1037nm. The absorption coefficient of hyperglycemia is at the same wavelength of 1037nm. Deoxyhemoglobin and oxyhemoglobin absorb light differently at frequencies spanning from 1000nm to 1200nm. At 900nm, permeation is more influential. The frequencies of perturbation can be monitored at two different frequencies: 905 nm and 1550 nm **[15]**. The regulated track's voltages (TTL trigger pulse) regulate the PLD output, allowing the pulse width and authority of the PLD to be adjusted during the operating condition. The TTL pulse is 100 Hz to excite an optical setup with a rising edge. A thermoelectric generator is used to acquire the photo-acoustic pulse, which is weak and accompanied by speckle variation. A reduced noise amplifier is used to boost the weak signal **[16]**. To increase the signal quality of the noisy signal, synchronous aggregating (parametric, diagnostic, or tensor aggregating) is applied. Coherence averaging reduces amplitude while preserving synchronous or coherent signal loudness. For synchronous aggregating, the amplitude of the information should be the same at the start of each reasoned sample set (intelligible averaging). The signal will aggregate to its real magnitude value once the time phase condition is met, and the clutter, which will not be the same in each specimen set, will aggregate to zero. The noninvasive hypoglycemia sensor to be utilized in this study to detect a quantity of glucose in our blood by detecting the concentration of high fructose corn syrup in our bodies, after which it is sent to the FPGA from before the before being communicated to the LCD and IoT.

Photo-acoustic technique

To modify the insulin levels, a transient laser beam (spectral illumination source) to 100s sinusoidal waveform and a burst intensity of 200 W is transmitted into the epithelium, leading to changes in the tissue's physics and refractive indices. These modifications aid in determining hyperglycemia. As shown in the equation, the subsequent intensity (I) of an acoustic wave is converted into the heat of light beam (F_0), absorption spectra modifier (γ), deformation (β), supersonic acceleration, and temperature gradient of increased

scrutiny (D_i) (1). The duration of the epithelium is among the predominant variables to consider (ρ_x), penetration intensity, epithelial optical transmittance at a frequency (γ). The sensor's heat transport distance, thermal diffusivity (TD), and attenuation amplitude (e) were indicated in calculations (2) and (3). Red light moisturizes to complexity from around 4.5mm **[18]**.

$$I = \frac{F_0 \gamma \delta U^2}{D_i} \quad (1)$$

$$\rho_x = \frac{1}{\gamma(\varepsilon)} \quad (2)$$

$$\rho_r = \frac{TD}{\pi e} \quad (3)$$

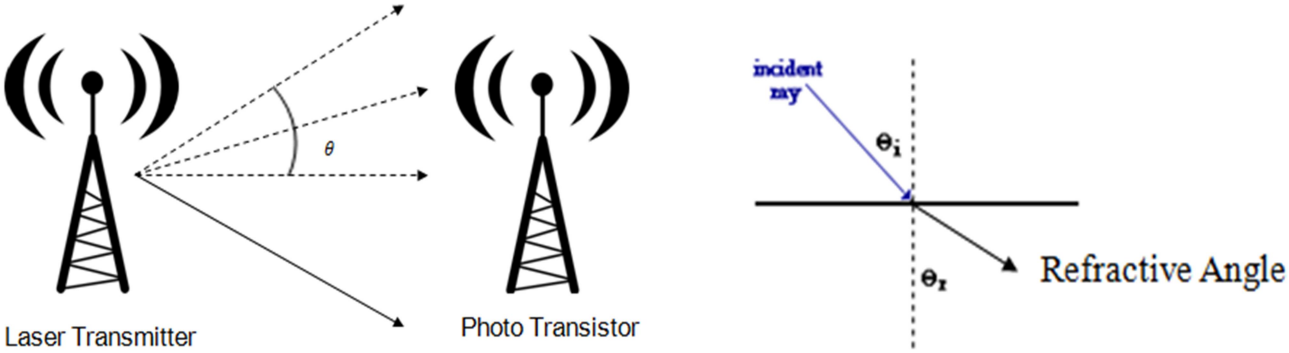

Figure 1 (a): Snell's law (b) It represents the link between plasma glucose and refractive angle

Figure 1 (a) shows the spectral slopes 1 (moisture) and 2 (air) (glucose). The elliptical optical point has an amplitude of πe , and the elliptical of the glucose concentration results is 'c. Equation (4) depicts the relationship (5).

The refractive index of the media and the optical angle of the light are both affected by starch content. Figure 1 depicts Snell's law that underpins this concept.

(b) Its assists in the approximation of n2 (fructose reflectivity). plasma glucose rises by 2 and reduces by 2 as illustrated in equation (6).

$$\theta_1 = \tan^{-1}\left(\frac{yz}{xz}\right) \quad (4)$$

$$\theta_2 = \tan^{-1}\left(\frac{y'z}{xz}\right) \quad (5)$$

$$m2 = \frac{m1(\sin\theta_1)}{(\sin\theta_2)} \quad (6)$$

Coherent and SN ratio

Since this transmission and noise spectra overlap, because the legitimate filtering process eliminates some transmitted evidence, standard filtration isn't employed to

tune out the noisy harmonics. Transmission aggregating is used to eliminate complexity and improve the transmitted pulse. The frequency half of transmission aggregating will tend to grow, but the acoustic half will be unstable and it will tend to cancel out. For synchronous aggregating to work, the transmitter magnitude should be the same at the start of each monitored sample group (time phase of the signal in each set to be identical). The presentation will aggregate to its actual magnitude when this criterion is met, and the noise within every total sample will be percentile to zero. To perform the service, it must be calibrated. In this study, they looked at 1024 various sampling sets. In every clip, a 1000 impulse is blended using speckle variation. The specimens of distortion are independent of one another as well as to the sampling frequency set 1 to 1000.

By following equation is derived from the above 1024 testing dataset by aggregating the Equation (7)

$$a_{average}(i) = \frac{1}{1024}\sum_{1024} am(i) = \frac{[a1(i) + a2(i) + a3(i) + \cdots \ldots + a1024(i)]}{1024} \quad (7)$$

which can be rephrase in the usual sequence

$a_{average}(1)$ =[$a_1(1)+a_2(1)+a_3(1)+\ldots+a_{1024}(1)$]/1024,

$a_{average}(2)$ =[$a_1(2)+a_2(2)+a_3(2)+\ldots+a_{1024}(2)$]/1024,

$a_{average}(3)$ = [$a_1(3)+a_2(3)+a_3(3)+\ldots+a_{1024}(3)$]/1024,…

$a_{average}(1000)$ = [$a_1(1)+a_2(1)+a_3(1)+\ldots+a_{1024}(1)$]/1024

x(n) is a transmission ($a_{average}(1)$) distorted by speckle variation, denoted by noise (n) and interpreted as x(n)= $a_{average}(1)$ +noise (For generate an appropriate figure of A, 1024 x(n) are aggregated to compute a discrete r approximate, which is illustrated in the Equation (8). The number of frames is N.

$$s_{avg(i)} = \frac{1}{M}\sum_{m=0}^{M} s([i-1].M + m) \quad (8)$$

$s_{avg(1)}$=[s(1)+r(2)+s(3)+…+r(1024)]/M ← 1 s t M (1024) point average

$s_{avg(2)}$ =[s(M+1)+s(M+2)+s(M+3)+…+s(2M)]/ ← 2nd M (1024) point average

$s_{avg(3)}$)=[s(2M+1)+s(2M+2)+s(2M+3)+…+s(3M)] ← 3rd M (1024) point average

To test if cohesive aggregating help reduces calibration, contrast the mean percentage deviation (k) and the r typical coefficient of determination (n). The transcendent signal's standard deviation (A) is σiin. As indicated in the equation, A particular structure's average packet drop proportion could be calculated (9). The equation is used to express the SNR of averaged frames (10). As seen in the figure, the method of coherence aggregating aids in increasing SNR (11). This total number measures the percentage of consecutive images.

$$Signal_{in} = \frac{X}{\alpha_{in}} \quad (9)$$

$$Signal_{avg} = \frac{s_{avg}}{\alpha_{avg}} = \frac{X}{\alpha_{avg}}$$

$$= \frac{X}{(\alpha_{in})/\sqrt{M}} \quad (10)$$

$$Signal_{CG} = \frac{s_{avg}}{s_{in}} \qquad Signal_{CG}$$

$$= \frac{[X/\alpha_{avg}]}{[X/\alpha_{in}]}$$

$$= \frac{\alpha_{in}}{(\alpha_{in})/\sqrt{M}} \quad (11)$$

$$Signal_{CG}$$

$$= \sqrt{M} \quad (12)$$

$$Signal_{CG}$$

$$= 10 \log 10 \, (\sqrt{M}) \quad (13)$$

Proposed method

The suggested system's framework is depicted in detail in **Figure 2**. In the proposed scheme, a limited amplifier is preceded by a modest ADC, FPGA, and LCD. To count the 1024 frames, and up monitor with 10 bits was employed. Because the architecture is reconfigurable, they can add more count bits if we need to count more than 1024 frames. This prompt encoder emits at amplitude TTL transmission, which takes into consideration each actionable activation wave, and every image is synchronized (ADC) with the initial frame to achieve a consistency average. To achieve a synchronized effect, Data in the register is used to impose a delay, allowing data to be collected accurately from the rising positive edge of the trigger signal. The PLD is initiated by the trigger generator. The management unit is controlled by the output of the 10 bit up counter. This microprocessor seems to be capable of identifying synthesizer & session encoder. All of the other blocks in the architecture generate a start signal from the counter. To write/read data into the Memory, the instructions write (w), read (r) and the select signal (rsel) are needed. RAM has a complexity of 1000 bytes and a breadth of 26 bytes. The address generator is in charge of generating the RAM access address. A parallelizing adder is used to combine reports collected in and passing out from the Memory (26 bit).

The Parallelizing adder **[19]** assists in the reduction of data route delays. The RAM is used to store arriving frames. The first frame is stored immediately in RAM, followed by the second through 1024 frames, which are stored one by one in RAMA supervisor transmits a stop signal to the counter when 1024 frames have been tallied, and coherent averaging is executed. To synthesize the analog signal, a 16 bit ADC (AD9265) is employed. The infrared component was triggered on if the enterprises are adopting prompt waves being transmitted. Every successful trigger pulse generates a photoacoustic signal in the tissue. A takes into account the incoming signals as frames and stores them one by one in the RAM. A three-clock-cycle delay is used to accomplish the parallelizing delay. RAM is primarily enabled for composing and then for reading and writing. Multiple synchronous cycles separate the Adrrd and Adrwr. When the refresh strength is increased, the regulator turns inside and starts up. The rsel frequency cycles from one to another (checkbox) through the period with the activate emitter wave. A frame is retrieved after this procedure. The rSel toggles after the first frame are taken, and the process is repeated until 1024 frames have been gathered, aggraded and coherent averaging has been completed.

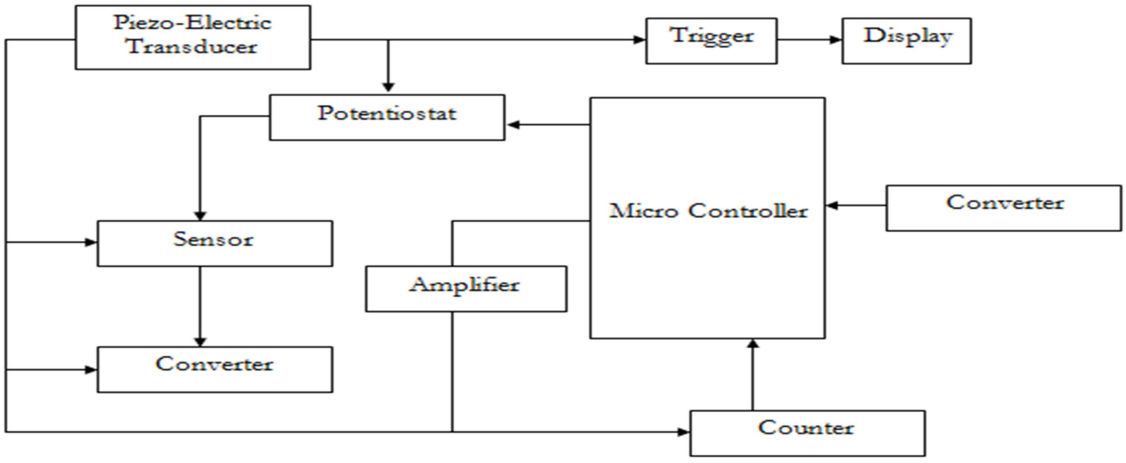

Figure 2: Coherence averaging and the suggested system

RESULTS AND DISCUSSION

The desired method is written in Verilog HDL and implemented on a Spartan-3 Xilinx FPGA. The modeling platform provides the theoretical values (modelsim). **Figure 3** depicts the photo-acoustic wave with speckle

variation. (a), while **Figure 3** depicts the coherence averaged signal. (b). To improve performance, device utilization statistics (ledger, retrieval columns, and arithmetic slices), timing settings, frequency band, and storage compatibility are used. The designed architecture's greatest operational frequency is 275 MHz, with an SNR of roughly 30 dB in a total of 1024 data. The proposed scheme has been able to dissipate, requiring only 110 milliwatts of power **[20]**. The implementation can be changed, and the number of data frames can be increased to improve reliability. A device will use IoT to deliver precise measurements and send emergency alerts, preventing unfavorable occurrences caused by excessive changes in hyperglycemia **[21-22]**. **Figure 4** shows a prototype of the suggested architecture (a). The PLD, transmitter and receiver circuits, FPGA, and LCD are all part of it. **Figure 4** depicts the architecture's IoT application (b). According to the synthesis reports, the quantity of slices used is quite low (110), and the quantity of flip-flops used is likewise very low (185). As a result, equipment use is very low, and the capacity factor is great.

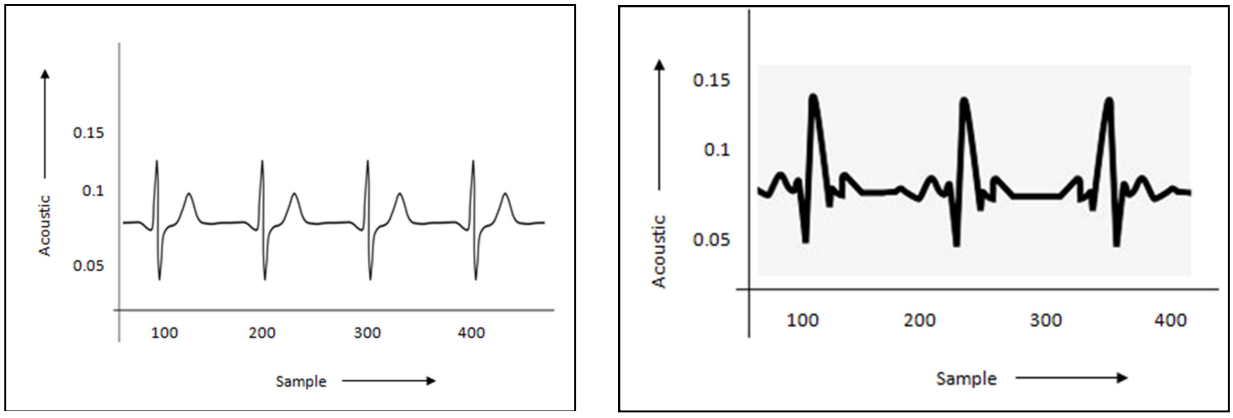

Figure 3 (a): Coherent average of 1024 signal with noise; (b) Optical acoustic signal with speckle variation

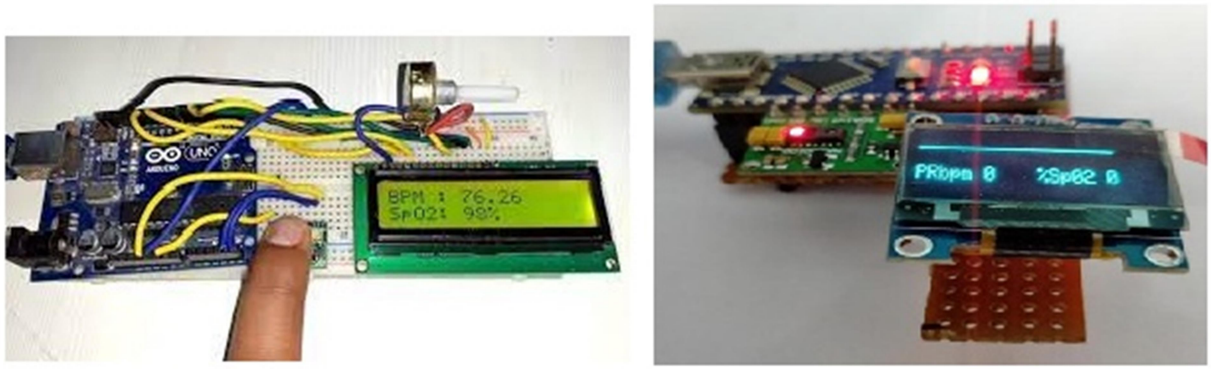

Figure 4 (a): Fabrication of such conceptual framework; (b) Fabrication about the intended system that makes use of the Internet of Things

CONCLUSION

The suggested architecture's velocity and area are both quite high, indicating that it performs well. Its design can be changed. Using consistent averaging, its design can be used to minimize random noise that has been tainted with the transmitter (Intelligible averaging). Mobile internet connections, data acquisition using biotelemetry, and satellite imagery are all possible with this framework. The planned architecture's IoT implementation has been realized. Patients requiring hyperglycemia monitoring on a daily or hourly basis will benefit from the noninvasive glucose monitoring device.

REFERENCES

[1] Ali, S. F., & Padhi, R. (2011). Optimal blood glucose regulation of diabetic patients using single network adaptive critics. *Optimal Control Applications and Methods*, *32*(2), 196-214.

[2] Bamgbose, S. O., Li, X., & Qian, L. (2017, October). Closed loop control of lood glucose level with neural network predictor for diabetic patients. In *2017 IEEE 19th International Conference on e-Health Networking, Applications and Services (Healthcom)* (pp. 1-6). IEEE.

[3] Charles, R. K. J., Mary, A. B., Jenova, R., & Majid, M. A. (2019). VLSI design of intelligent, Self-monitored and managed, Strip-free, Non-invasive device for Diabetes mellitus patients to improve Glycemic control using IoT. *Procedia Computer Science*, *163*, 117-124.

[4] Dr. P. Sivakumar, "Analytical framework to build predictive and optimization function from manufacturing industry sensor data using cross-sectional sharing", Big Data,2021 (SCI)

[5] Dr. P. Sivakumar, "Improved Resource management and utilization based on a fog-cloud computing system with IoT incorporated with Classifier systems", Microprocessors and Microsystems, Jan 2021 (SCI).

[6] Ranjeeth, S., Latchoumi, T. P., & Paul, P. V. (2020). Role of gender on academic performance based on different parameters: Data from secondary school education. Data in brief, 29, 105257.

[7] Venkata Pavan, M., Karnan, B., & Latchoumi, T. P. (2021). PLA-Cu reinforced composite filament: Preparation and flexural property printed at different machining

conditions. Advanced Composite Materials, https://doi.org/10.1080/09243046.2021, 1918608.

[8] Buda, R. A., & Addi, M. M. (2014, December). A portable non-invasive blood glucose monitoring device. In *2014 IEEE Conference on Biomedical Engineering and Sciences (IECBES)* (pp. 964-969). IEEE.

[9] Delbeck, S., Vahlsing, T., Leonhardt, S., Steiner, G., & Heise, H. M. (2019). Non-invasive monitoring of blood glucose using optical methods for skin spectroscopy—opportunities and recent advances. *Analytical and bioanalytical chemistry*, *411*(1), 63-77.

[10] Steiner, M. S., Duerkop, A., & Wolfbeis, O. S. (2011). Optical methods for sensing glucose. *Chemical Society Reviews*, *40*(9), 4805-4839.

[11] Jernelv, I. L., Milenko, K., Fuglerud, S. S., Hjelme, D. R., Ellingsen, R., & Aksnes, A. (2019). A review of optical methods for continuous glucose monitoring. *Applied Spectroscopy Reviews*, *54*(7), 543-572.

[12] Zhang, J., Taniguchi, T., Takita, T., & Ali, A. B. (2003). A study on the epidermal structure of Perioph-thalmodon and Periophthalmus mudskippers with reference to their terrestrial adaptation. *Ichthyological Research*, *50*(4), 310-317.

[13] Kobuchi, S., Kabata, T., Maeda, K., Ito, Y., & Sakaeda, T. (2020). Pharmacokinetics of macrolide antibiotics and transport into the interstitial fluid: comparison among erythromycin, clarithromycin, and azithromycin. *Antibiotics*, *9*(4), 199.

[14] Nahavandi, P. (2020). *Developing novel non-invasive MRI techniques to assess cerebrospinal fluid-interstitial fluid (CSF-ISF) exchange* (Doctoral dissertation, UCL (University College London)).

[15] Paul, M. C., Kir'yanov, A. V., Barmenkov, Y., Duarte, J., Leitão, J. P., Ferreira, M. F., & Dutta, D. A new class of specialty optical fibers based on a novel material composition of the doping host for the study of optical amplification.

[16] Bednarkiewicz, A., Marciniak, L., Carlos, L. D., & Jaque, D. (2020). Standardizing luminescence nanothermometry for biomedical applications. *Nanoscale*, *12*(27), 14405-14421.

[17] Perrot, V., Polichetti, M., Varray, F., & Garcia, D. (2021). So you think you can DAS? A viewpoint on delay-and-sum beamforming. *Ultrasonics*, *111*, 106309.

[18] Fast, A., Lal, A., Durkin, A. F., Lentsch, G., Harris, R. M., Zachary, C. B. & Balu, M. (2020). Fast, large area multiphoton exoscope (FLAME) for macroscopic imaging with microscopic resolution of human skin. *Scientific reports*, *10*(1), 1-14.

[19] Chen, T. L., Lin, Y. P., Chien, C. H., Chen, Y. C., Yang, Y. J., Wang, W. L., ... & Hsueh, H. Y. (2021). Fabrication of Frog-Skin-Inspired Slippery Antibiofouling Coatings Through Degradable Block Copolymer Wrinkling. *Advanced Functional Materials*, 2104173.

[20] Jones, P. (2020). *Bodies, Technologies and Methods*. Routledge.

[21] Gerhard Nahler, N. (2020). Dictionary of Pharmaceutical Medicine.

[22] Ofri, D. (2020). *When we do harm: a doctor confronts medical error*. Beacon Press.